Journal of Porphyrins and Phthalocyanines
J. Porphyrins Phthalocyanines 2023; **27**: 1241–1252
DOI: 10.1142/S1088424623500840

Published at https://www.worldscinet.com/jpp/

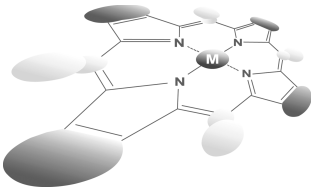

Synthesis and optical properties of 3,5-bis(10-phenylanthracen-9-yl)benzene-appended porphyrins

Akane Umemiya[a], Haruyuki Nakano[b], Nanami Iwaya[c], Tadaaki Ikoma[c], and Yoshihiro Matano[◊,*,c]

[a]*Department of Fundamental Sciences, Graduate School of Science and Technology, Niigata University, Nishi-ku, Niigata 950-2181, Japan*
[b]*Department of Chemistry, Graduate School of Science, Kyushu University, Nishi-ku, Fukuoka 819-0395, Japan*
[c]*Department of Chemistry, Faculty of Science, Niigata University, Nishi-ku, Niigata 950-2181, Japan*

Received 16 January 2023
Accepted 16 March 2023

Dedicated to Prof. Jonathan L. Sessler on the occasion of his 65th birthday

ABSTRACT: Singlet–singlet and triplet-triplet energy-transfer processes between anthracenes and porphyrins have received considerable attention in materials chemistry. Herein, we report the first examples of 3,5-bis(10-phenylanthracen-9-yl)benzene-appended porphyrins (BPABPs) designed to study intramolecular energy transfer between two chromophores. The Curtius rearrangement of 3,5-bis(10-phenylanthracen-9-yl)benzoyl azide in the presence of the platinum(II) complex of 5,10,15-tris(3,5-di-*tert*-butylphenyl)-20-(3-hydroxyphenyl)porphyrin or its free base in toluene afforded the corresponding BPABP. Spectroscopy, cyclic voltammetry, and density functional theory calculations revealed that the anthracene and porphyrin π-electron systems of the BPABPs are not conjugated and consequently do not affect each other's absorption properties. In contrast, the BPABPs exhibited considerably different luminescence properties to those of phenyl 3,5-bis(10-phenylanthracen-9-yl)carbamate and 5,10,15-tris(3,5-di-*tert*-butylphenyl)-20-(3-methoxyphenyl)porphyrins; the anthracene units of the BPABPs show considerably quenched fluorescence compared to that of the reference anthracene, indicative of efficient intramolecular singlet–singlet energy transfer from the anthracene to the porphyrin unit. The phosphorescence quantum yield of the Pt complex of BPABP is comparable to that of the reference Pt-porphyrin, which suggests that intramolecular triplet-triplet energy transfer from the Pt-porphyrin to the anthracene unit is inefficient. The present findings improve our understanding of how structural factors and excited-state energy levels affect energy transfer and triplet-triplet annihilation upconversion processes of covalently linked bisanthracene-appended porphyrins.

KEYWORDS: porphyrin, anthracene, fluorescence, phosphorescence, triplet-triplet annihilation

INTRODUCTION

Singlet–singlet and triplet-triplet energy-transfer processes between anthracenes and porphyrins have been extensively investigated in the materials chemistry field [1]. For example, much attention has been paid to triplet-triplet annihilation upconversion (TTA-UC) phenomena in photovoltaics [2], photoredox catalysis [3], bio-imaging [4], and photodynamic therapy [5] applications. TTA-UC is a bimolecular photophysical process that generates one high-energy excited state (emissive exciton) from two low-energy triplet states (dark excitons) and typically proceeds according to the following steps: (1) Irradiation of the sensitizer generates the excited triplet (T_1) state via intersystem crossing from the excited singlet (S_1) state; (2) triplet-triplet energy transfer from the

[◊]SPP full member in good standing.

*Correspondence to: Yoshihiro Matano, Department of Chemistry, Faculty of Science, Niigata University, Nishi-ku, Niigata 950-2181, Japan; Tel: +81-25-262-7734; Fax: +81-25-262-7734; E-mail: matano@chem.sc.niigata-u.ac.jp

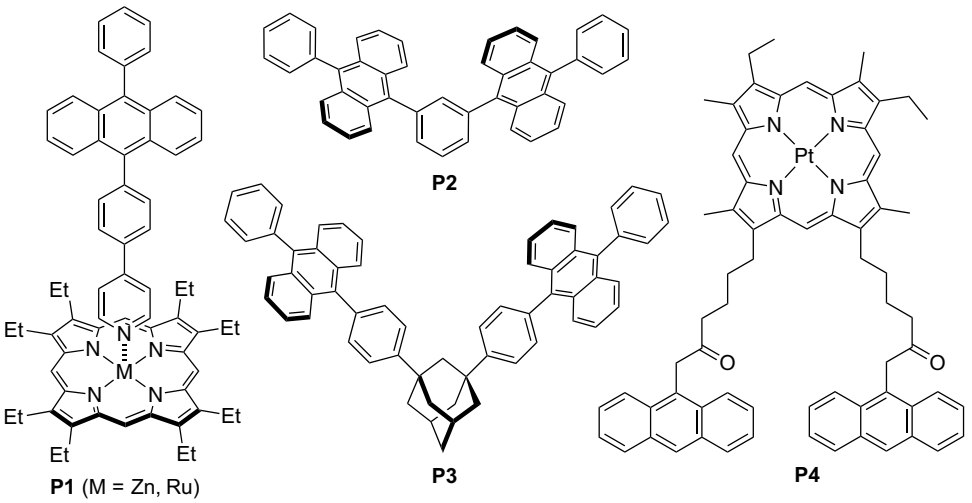

Chart 1. Previously reported compounds **P1**–**P4**.

sensitizer to the annihilator generates the T_1 state of the annihilator; (3) two T_1-state annihilator molecules collide and split into an S_1 state and an S_0 state. Consequently, the S_1 state of the annihilator fluoresces at a frequency higher than that of the incident light. 9,10-Disubstituted anthracenes and metal complexes of porphyrins have been used as annihilators and sensitizers, respectively, in many TTA-UC systems because their S_1 and T_1 energy levels are appropriate for studying this phenomenon [1, 6]. Understanding how the distance and orientation between these chromophores affect energy-transfer efficiency is a key challenge for improving the TTA-UC efficiency of an anthracene–porphyrin system. A promising way to achieve this is to link the sensitizer and annihilator or connect the multiple annihilators [7–12]. For example, Albinsson and coworkers synthesized anthracene–porphyrin dyads **P1** (Chart 1) to investigate intramolecular energy-transfer processes and TTA–UC mechanisms in solution and discussed the factors that limit this coordinating annihilator-sensitizer systems [9]. Albinsson *et al*. [10b] and Ikeda *et al*. [10a] independently studied TTA-UC using cleverly designed phenylene- and adamantane-linked 9,10-diphenylanthracene (DPA) dyads **P2** and **P3**, respectively, as annihilators and 2,3,7,8,12,13,17,18-octaethylporphyrinatoplatinum(II) (PtOEP) as an external sensitizer. However, little attention has been paid to the optical properties and energy-transfer behavior of covalently linked bisanthracene–porphyrin triads due to the limited number of such examples [11, 12]. Recently, Tanaka *et al*. reported that dual anthracene-tethered porphyrin **P4** with mobile alkyl-chain linkers play significant roles in producing higher-energy photons by mediating intermolecular energy transfer from the Pt-porphyrin unit to free anthracene [11b]. We envisaged that the use of peripherally functionalized porphyrins containing two DPA units with defined distance and orientation would facilitate investigating the effect of structure on intramolecular energy transfer among the three chromophores. Herein, we report the first examples of 3,5-bis(10-phenylanthracen-9-yl)benzene-appended porphyrin (BPABP) as a platinum(II) complex and a free base. The optical properties and TTA-UC phenomena of these BPABPs and reference dyes were investigated.

RESULTS AND DISCUSSION

The BPABPs and reference dyes were synthesized as summarized in Scheme 1. A mixture of 5-(3,5-di-*tert*-butyl)phenyldipyrromethane (**1**), 5-(3-methoxyphenyl) dipyrromethane (**2**), and 3,5-di-*tert*-butylbenzaldehyde (**3**) was treated with BF_3•OEt_2 in CH_2Cl_2 for 1 h at room temperature, after which 2,3-dichloro-5,6-dicyanobenzoquinone (DDQ) was added. Silica-gel column chromatography of the reaction mixture afforded 5,10,15-tris(3,5-di-*tert*-butylphenyl)-20-(3-methoxyphenyl)porphyrin (**4H$_2$**) as a purple solid. A mixture of free base **4H$_2$** and $Pt(acac)_2$ (acac = acetylacetonato) was subsequently heated in boiling benzonitrile to afford platinum(II) complex **4Pt** as an orange solid. *meso*-(3-Methoxyphenyl)-porphyrins **4M** (M = H_2 and Pt) were quantitatively *O*-demethylated using BBr_3 in CH_2Cl_2 to afford the corresponding *meso*-(3-hydroxyphenyl)-porphyrins **5M** (M = H_2 and Pt). The *meta*-phenylene-bridged bis(anthracene) derivative **8** was prepared by the Suzuki-Miyaura coupling of methyl 3,5-dibromobenzoate (**6**) with (10-phenylanthracen-9-yl)boronic acid (**7**) in the presence of a catalytic amount of $Pd(PPh_3)_4$ and K_2CO_3 in a mixed solvent system. Alkaline hydrolysis of the ester group in **8** yielded carboxylic acid **9**; subsequent sequential treatment with $SOCl_2$ and NaN_3 yielded acyl azide **10**, which was spectroscopically characterized and used in the next reaction without purification. The target BPABPs **11M** (M = H_2 and Pt) were prepared by heating a toluene solution of **10**, **5M**, and triethylamine for several hours at 110 °C, during which the isocyanate intermediate generated by the Curtius rearrangement of

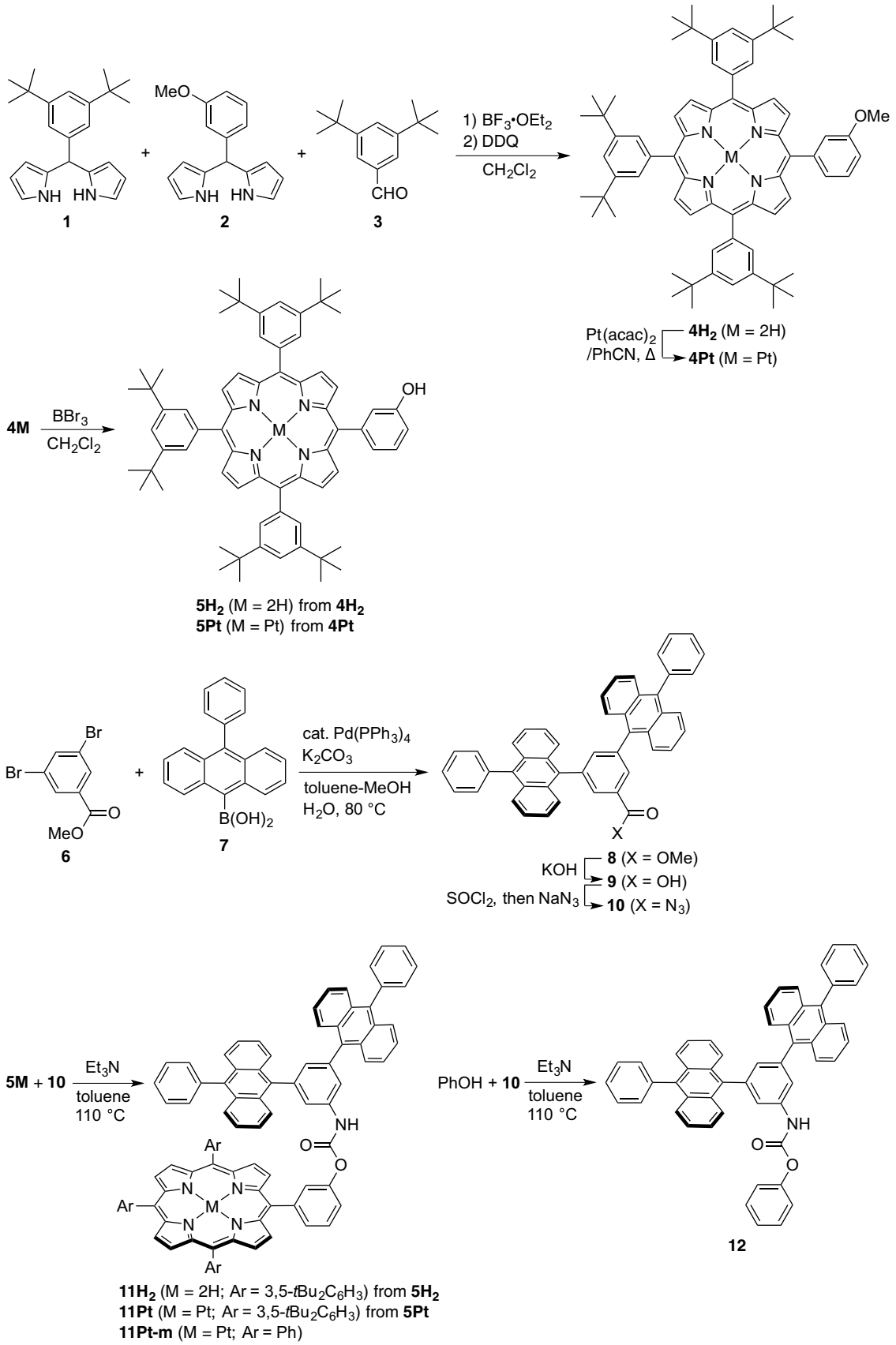

Scheme 1. Synthesis of BPABPs **11M** and their reference compounds.

10 was trapped by the 3-hydroxyphenyl group of **5M** to form a carbamate linkage. Reference bisDPA **12** was obtained when phenol was reacted with **10** under the same conditions.

The new compounds were characterized by NMR spectroscopy, IR spectroscopy, and high-resolution electrospray mass spectrometry (HR-ESIMS). The HR-ESIMS spectra of BPABPs **11Pt** and **11H$_2$** showed molecular ion peaks at *m/z* values of 1783.7964 and 1591.8543 ([M + H]$^+$), respectively. The IR spectra of carbamates **11M** and **12** display N–H/C=O stretching bands at ν_{max} values of 1749/3393 and 1753/3399 cm^{-1}, respectively. The ^{1}H NMR spectra of **4Pt**, **11Pt**, and **12** are shown in Fig. 1. The pyrrolic-β protons of **4Pt** and **11Pt** appear in the same region (8.8–8.7 ppm), while the anthracene ring protons in **11Pt** are affected by a tiny ring current from the porphyrin ring. These data indicate that the porphyrin and anthracene π-electron systems of **11Pt** effectively do not interact spatially; the same is true for the free base **11H$_2$**. The anthracene ring protons of BPABPs **11M** appear to be equivalent, which suggests that the BPAB unit can freely rotate around the C–N and/or C–O single bond on the NMR timescale.

The structure of **11Pt-m** (depicted in Scheme 1) was optimized using density functional theory (DFT) to provide information about the relative geometry of the three chromophores in triad **11Pt**. Stable conformer searching was performed by rotating the BPAB unit around the *ipso*-C–O bond axis, which yielded two structures that differed in energy by only 0.13 kcal mol^{-1}. One of the structures (conformer A) is shown in Fig. 2, with the other (conformer B) shown in Figure S1 (Supporting Information) together with selected Kohn-Sham orbitals.

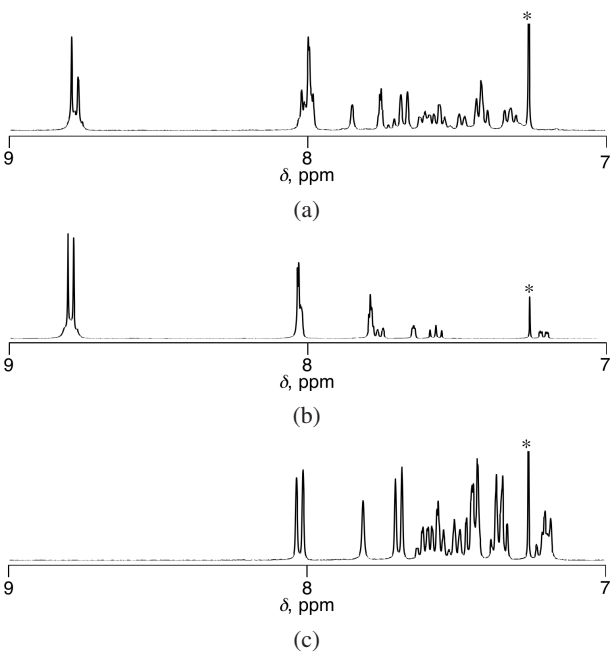

Fig. 1. ^{1}H NMR spectra (400 MHz; 9–7 ppm) of (a) **11Pt**, (b) **4Pt**, and (c) **12** in $CDCl_3$. Asterisk indicates the residual $CHCl_3$.

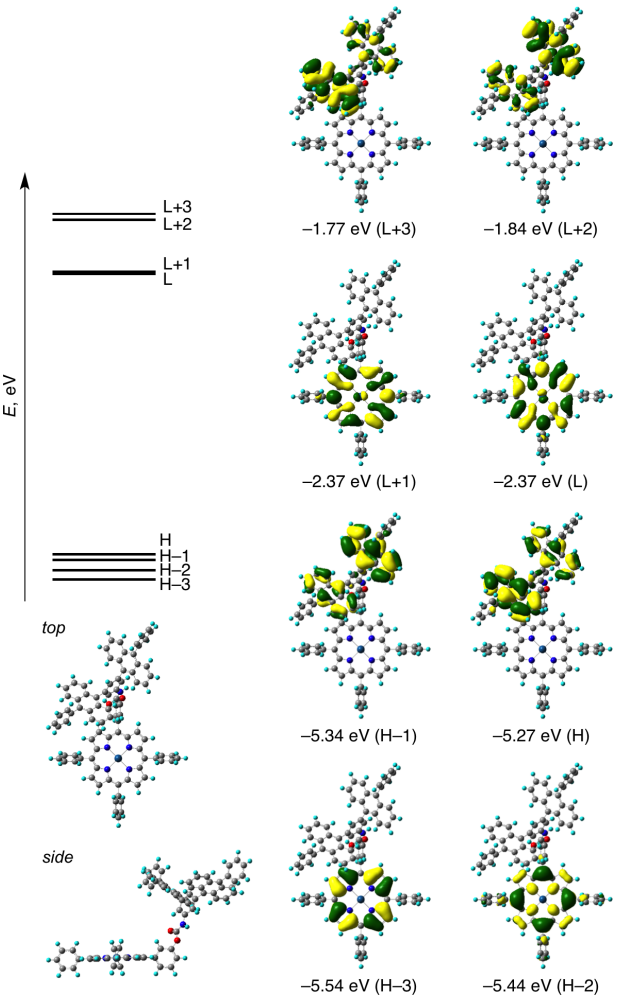

Fig. 2. Selected Kohn-Sham orbitals and their energies (in eV) of **11Pt-m** (conformer A) were calculated by the DFT method with the solvent effect (PCM, CH_2Cl_2). H = HOMO, L = LUMO.

The rotational barrier connecting conformers A and B was roughly determined to be 9 kcal mol^{-1}, which is sufficiently small to enable the BPAB unit to rotate freely around the *ipso*-C–O bond axis at room temperature (Fig. S2). The *meso*-aryl group linked to the BPAB unit in each conformer is highly twisted against the porphyrin ring, with a torsion angle of 57.5–62.3°, suggestive of negligible resonance between the BPAB and porphyrin units. The anthracene units are significantly twisted against the phenylene spacer, which implies that the two anthracene π-electron systems are poorly conjugated. Conformer A exhibits distances of about 11.6 Å and 14.8 Å from the Pt center to the *ipso* carbon at position-9 of the inner and outer anthracene rings, respectively.

The electrochemical properties of **4M**, **11M**, and **12** were assessed by measuring their redox potentials in CH_2Cl_2 using cyclic voltammetry (CV) with Bu_4NPF_6 as the supporting electrolyte (Fig. 3 and Table 1). Triads **11M** exhibited several reversible redox processes centered at E = −1.80 (1e), +0.64 (1e), and +0.72 (2e) V for

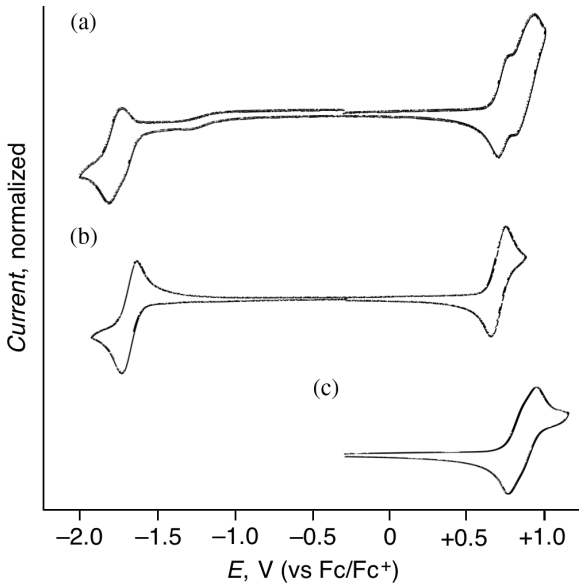

Fig. 3. Cyclic voltammograms of (a) **11Pt**, (b) **4Pt**, and (c) **12** in CH_2Cl_2 with Bu_4NPF_6 as a supporting electrolyte. Scan rate = 60 mV s^{-1}.

11Pt, and −1.76 (1e), +0.48 (1e), and +0.79 (2e) V for **11H$_2$** (vs. the ferrocene/ferrocenium couple; Fc/Fc^+). The one-electron processes at −1.80/−1.76 and +0.64/+0.48 V are assigned to porphyrin-ring-centered redox couples by comparison with the voltammograms of the corresponding reference porphyrins **4M**. The $E_{1/2}$ values of **11M** are almost identical to those of **4M** and **12**, which indicates that the porphyrin and BPAB units of **11M** essentially do not affect each other's electrochemical properties [13].

The ultraviolet/visible (UV/Vis) absorption and emission spectra of **4M**, **11M**, and **12** in CH_2Cl_2 are shown in Fig. 4 and the optical data are summarized in Table 1. A Soret and two Q bands, with absorption maxima (λ_{abs}) at 405 and 511/540 nm, respectively, are observed in the absorption spectrum of **11Pt** (Fig. 4a), whereas anthracene-based π–π* electronic transitions are observed as shoulders in the UV region. The λ_{abs} values of the Soret and Q bands of **11Pt** are very close to those of the reference Pt-porphyrin **4Pt** (Fig. 4b; λ_{Soret} = 404, λ_Q = 511/540 nm), suggesting that the BPAB unit has a negligible through-bond electronic effect on the porphyrin-based π–π* excitation energies. The same is true for **11H$_2$** (Fig. 4d), which exhibits a Soret band (λ_{abs} = 420 nm) and four Q bands (λ_{abs} = 518/552/591/647 nm) at almost the same wavelengths as those of **4H$_2$** (Fig. 4e; λ_{Soret} = 420 nm, λ_Q = 517/553/591/647 nm).

Figures 2 and S1 show that the highest occupied molecular orbitals (HOMO and HOMO−n; n = 1–3) and lowest unoccupied molecular orbitals (LUMO and LUMO+n; n = 1–3) of **11Pt-m** are distributed over the Pt-porphyrin ring or the two anthracene rings of the BPAB unit and that the anthracene-based HOMOs and LUMOs are essentially degenerate. The anthracene-based HOMOs (HOMO and HOMO−1) are slightly higher in energy than the porphyrin-based HOMOs (HOMO−2 and HOMO−3), which is inconsistent with the experimental data obtained by CV (vide supra), although the reason for this discrepancy is not clear at present. The electronic transition energies of **11Pt-m** were calculated using time-dependent DFT (TD-DFT), the results of which are summarized in Table 2. The lower-energy porphyrin-based transitions (from HOMO−2/HOMO−3 to LUMO/LUMO+1; states 1 and 2) are symmetrically forbidden, which is characteristic of typical porphyrin Q bands, whereas higher-energy porphyrin-based transitions (states 15 and 16) correspond to symmetrically allowed Soret bands. Excited states 10–12 involve π–π* transitions involving the two anthracene chromophores. These assignments qualitatively explain the experimentally observed UV/Vis absorption spectra of **11Pt**.

The photoluminescence (PL) spectrum of **11Pt** in CH_2Cl_2 when excited at 404 nm at room temperature exhibits dual emissions with maxima (λ_{em}) at 674/746 and 415/433 nm (Fig. 4a), in good agreement with the phosphorescence of **4Pt** (Fig. 4b; λ_{em} = 674/744 nm) and the fluorescence of **12** (Fig. 4c; λ_{em} = 412/433 nm), respectively. The PL spectrum of **11Pt** shows the same long-wavelength emission when excited at 511 nm. The excitation spectrum of **11Pt** monitored at λ_{em} = 675 nm is well matched to its absorption spectrum. These results indicate that the higher- and lower-energy PLs of **11Pt** correspond to anthracene-derived fluorescence and Pt-porphyrin-derived phosphorescence, respectively. The

Table 1. Optical and electrochemical data for **4M**, **11M**, and **12**.[a]

Compd	λ_{abs} [nm][b]	λ_{em} [nm][c] (Φ_{em}[d]; τ_p[e])	$E_{1/2}$ [V][f]
4Pt	404, 511, 540	674, 744 (<0.01; 0.66 μs)	−1.83, 0.64
4H$_2$	420, 517, 553, 591, 647	653, 721 (0.07)	−1.73, 0.45
11Pt	405, 511, 540	415, 433, 674, 746 (<0.01; 0.93 μs)	−1.80, 0.64, 0.72
11H$_2$	376, 420, 518, 552, 591, 647	411, 434, 653, 721 (0.06)	−1.76, 0.48, 0.79
12	357, 377, 398	412, 433 (0.91)	0.76, 0.81

[a]Measured in CH_2Cl_2. [b]Absorption maxima. [c]Emission maxima: λ_{ex} = 511 nm (**4Pt**), 516 nm (**4H$_2$**), 404, 511 nm (**11Pt**), 376, 518 nm (**11H$_2$**), 398 nm (**12**). [d]Absolute emission quantum yields: λ_{ex} = 400 nm (**4Pt**), 420 nm (**4H$_2$**), 380, 400 nm (**11Pt**), 395, 420 nm (**11H$_2$**), 380 nm (**12**). [e]Phosphorescence lifetimes of **4Pt** and **11Pt**: λ_{ex} = 532 nm. [f]Redox potentials (half-wave potentials vs. Fc/Fc^+) determined by CV and DPV.

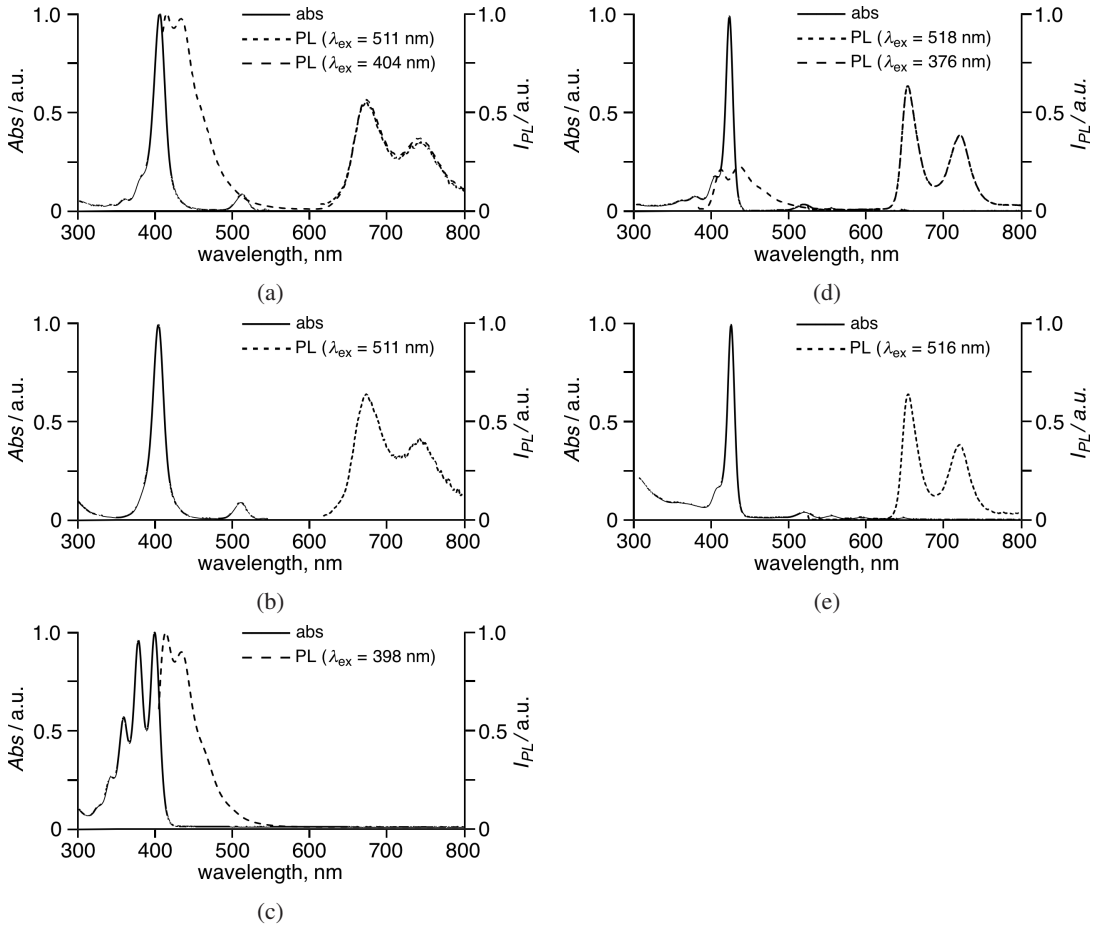

Fig. 4. UV/Vis absorption (solid line) and emission (dotted line) spectra of (a) **11Pt**, (b) **4Pt**, (c) **12**, (d) **11H$_2$**, and (e) **4H$_2$** in CH_2Cl_2.

Table 2. Excitation energies and oscillator strengths of **11Pt-m** were calculated by the TD-DFT method.[a]

State	Excitation energy [eV/nm] (Oscillator strength)	Excitation (Weight [%])
	Conformer A	
1	2.48/499.6 (0.006)	HOMO−2 –> LUMO (51.3), HOMO−3 –> LUMO+1 (42.5)
2	2.48/499.2 (0.006)	HOMO−2 –> LUMO+1 (50.7), HOMO−3 –> LUMO (43.0)
10	3.05/407 (0.178)	HOMO –> LUMO+2 (97.8)
11	3.12/397 (0.079)	HOMO−1 –> LUMO+2 (51.5), HOMO –> LUMO+3 (45.6)
12	3.15/394 (0.226)	HOMO –> LUMO+3 (49.3), HOMO−1 –> LUMO+2 (43.8)
15	3.20/387.9 (1.298)	HOMO−3 –> LUMO (33.0), HOMO−2 –> LUMO+1 (27.6)
16	3.20/387.5 (1.370)	HOMO−3 –> LUMO+1 (36.8), HOMO−2 –> LUMO (30.0)
	Conformer B	
1	2.48/499.9 (0.008)	HOMO−2 –> LUMO (54.5), HOMO−3 –> LUMO+1 (44.4)
2	2.48/499.5 (0.005)	HOMO−2 –> LUMO+1 (53.5), HOMO−3 –> LUMO (45.4)
10	3.04/407 (0.200)	HOMO –> LUMO+2 (97.8)
11	3.12/398 (0.074)	HOMO−1 –> LUMO+2 (50.7), HOMO –> LUMO+3 (46.6)
12	3.14/394 (0.309)	HOMO –> LUMO+3 (49.2), HOMO−1 –> LUMO+2 (44.8)
15	3.19/388.1 (1.364)	HOMO−3 –> LUMO (50.6), HOMO−2 –> LUMO+1 (42.2)
16	3.20/387.9 (1.327)	HOMO−3 –> LUMO+1 (49.4), HOMO−2 –> LUMO (39.6)

[a]B3LYP/6-311G(d,p) and Wachters–Hay(f) (PCM, CH_2Cl_2) at the optimized structures. Except for states 1 and 2, the states whose oscillator strengths are less than 0.07 are not included.

PL spectrum of **11H$_2$** also shows dual emissions (Fig. 4d; λ_{em} = 653/721 and 411/434 nm) assigned to fluorescence from the H_2-porphyrin and anthracene units, respectively, upon comparison with the PL spectra of **4H$_2$** (Fig. 4e) and **12** (Fig. 4c). From the experimentally observed absorption and emission spectra of **11Pt** and its reference dyes in CH_2Cl_2, the S_2, S_1, and T_1 energy levels of the Pt-porphyrin unit in **11Pt** and **4Pt** are determined to be 3.0, 2.3, and 1.8 eV, respectively, whereas the S_1 energy level of the BPAB unit in **11Pt** is determined to be 3.1 eV. Similarly, the S_2 and S_1 energy levels of the H_2-porphyrin unit in **11H$_2$** are determined to be 2.9 and 1.9 eV, respectively, whereas the S_1 energy level of the BPAB unit in **11H$_2$** is determined to be 3.1 eV. Phosphorescence from the BPAB units in **11M** and **12** could not be detected under the measurement conditions; hence the T_1 energy level reported for DPA (1.77 eV) [14] is used in the following discussion.

To gain some insight into the energy-transfer processes from the excited **11M**, absolute PL quantum yields (Φ_{em}) of **4M**, **11M**, and **12** and lifetimes (τ_p) of **4Pt** and **11Pt** were measured at room temperature, the results of which are summarized in Table 1. The Φ_{em} values of the higher-energy anthracene-derived fluorescence of **11Pt** and **11H$_2$** (<0.01 each; λ_{ex} = 380–395 nm) are very low compared to that of **12** (0.91; λ_{ex} = 380 nm), consistent with significantly quenched fluorescence from the BPAB unit of **11M**; hence, Förster-type resonance energy transfer from the anthracene to the porphyrin unit appears to occur efficiently in **11M**. Pt-porphyrins **11Pt** and **4Pt** exhibit comparable very low phosphorescence quantum yields (Φ_{em} <0.01) and short phosphorescence lifetimes (τ_p = 0.66–0.93 μs) compared to the corresponding values of 5,10,15,20-tetraphenylporphyrinatoplatinum(II) (PtTPP; Φ_e = 0.046; τ_p = 59 μs in CH_2Cl_2 at 298 K) [15]. These results indicate that the triplet-triplet energy transfer from the Pt-porphyrin to the anthracene unit of **11Pt** is inefficient. This is probably ascribable to (i) fast nonradiative decay from the T_1 to S_0 state due to the substituents of the *meso*-aryl groups, (ii) the relatively long distances between the porphyrin ring and anthracene moieties in **11Pt**, and/or (iii) the inappropriate combination of the triplet energy levels of the Pt-porphyrin and DPA chromophores (vide infra). These factors reduce triplet-triplet energy-transfer efficiency by the Dexter mechanism.

Finally, we attempted to observe the fluorescence of DPA or DPA chromophore derived from TTA-UC using sensitizers (**4Pt**, PtOEP), annihilators (**12**, DPA), and BPABP **11Pt**. Upon excitation with visible light at 511 nm, deaerated CH_2Cl_2 solutions of **4Pt/12** (20/400 μM) and **4Pt**/DPA (20/400 μM) displayed only very weak fluorescence in the range of 380–460 nm (Figs. S3a, S3b), indicating that TTA-UC does not proceed efficiently in these solutions. Under the same measurement conditions, CH_2Cl_2 solutions of PtOEP/**12** (20/400 μM) and PtOEP/DPA (20/400 μM) exhibited DPA-derived fluorescence (Figs. S3c, S3d), the intensity of which varied depending on the concentration of the sensitizer. This observation indicates that TTA-UC proceeds in the binary systems when PtOEP is used as the sensitizer. The poor TTA-UC efficiency of the **4Pt**/DPA binary system may be due to the low T_1 energy level of **4Pt** (1.8 eV) compared to PtOEP (1.9 eV). It was hardly detectable DPA-derived fluorescence through intramolecular TTA-UC of BPABP **11Pt** under the present measurement conditions (Fig. S3e). These results suggest that more detailed measurements, such as changes in excitation light intensity, are required to further investigate intramolecular TTA-UC phenomena using covalently linked bisDPA–porphyrin triads.

In summary, we synthesized the first examples of BPABPs through the Curtius rearrangement of 3,5-bis(10-phenylanthracen-9-yl)benzoyl azide in the presence of the corresponding 3-hydroxyphenyl-appended porphyrins. Spectroscopy, cyclic voltammetry, and DFT calculations revealed that the anthracene and porphyrin units of the BPABPs are spatially separated and unconjugated. The UV/Vis absorption spectra of the BPABPs in CH_2Cl_2 exhibit characteristic absorption bands that correspond to π–π* electronic transitions derived from their anthracene and porphyrin chromophores, while the UV/Vis luminescence spectra reveal anthracene-derived fluorescence and porphyrin-derived phosphorescence (for the Pt complex) or fluorescence (for the free base). However, the anthracene-based BPABP fluorescence was significantly quenched by the neighboring porphyrin units. These results indicate that intramolecular singlet–singlet energy transfer from the anthracene to the porphyrin unit occurs efficiently in these BPABPs. In contrast, the Pt-porphyrin-derived phosphorescence of BPABP was not significantly quenched by the anthracene units, consistent with insufficient intramolecular triplet-triplet energy transfer from the porphyrin to the anthracene unit. This study improves our understanding of how structural factors and excited-state energy levels affect energy transfer and TTA-UC processes of covalently linked bisanthracene-appended porphyrins. Studies aimed at further evaluating the excited-state dynamics of BPABPs and related compounds are ongoing.

EXPERIMENTAL

General

All melting points were recorded on a Yazawa micro melting point apparatus and are uncorrected. ^{1}H NMR and $^{13}C\{^1H\}$ NMR spectra were recorded on a Bruker 400 MHz spectrometer using $CDCl_3$ as a solvent. Chemical shifts are reported as relative values vs tetramethylsilane. High-resolution electrospray mass spectra (HR-ESIMS) were obtained on a Thermo Fisher Scientific EXACTIVE spectrometer. UV/Vis absorption and emission spectra were measured at room temperature on JASCO V-530 and EP-8300 spectrometers, respectively.

IR (Attenuated Total Reflection; ATR) spectra were obtained on a JASCO FT/IR4600 spectrometer. Absolute fluorescence quantum yields were measured on a Hamamatsu Photonics Quantaurus-QY spectrometer. Thin-layer chromatography was performed with Alt. 5554 DC-Alufolien Kieselgel 60 F254 (Merck), and preparative column chromatography was performed using Silica Gel 60 spherical, neutrality (Nacalai tesque). All reactions were performed under an argon or nitrogen atmosphere. Compounds **1** [16], **2** [17], and **3** [18] were prepared according to the literature methods. Compound **7** was prepared from 9-bromo-10-phenylanthracene via lithiation. Other chemicals and solvents were of reagent-grade quality and used without further purification unless otherwise noted. The synthetic procedures and characterization data of new compounds are described below. The IR, mass, and ^{1}H NMR spectra are shown in the Supporting Information.

Synthesis and Characterization

5,10,15-Tris(3,5-di-tert-butylphenyl)-20-(3-methoxyphenyl)porphyrin (4H$_2$). A mixture of **1** (532 mg, 1.59 mmol), **2** (406 mg, 1.61 mmol), **3** (695 mg, 3.18 mmol), and CH_2Cl_2 (350 mL) was deoxygenated by bubbling argon gas for 20 min, followed by the dropwise addition of BF_3•OEt_2 (120 μL, 0.955 mmol), and the resulting mixture was stirred for 1 h at room temperature. DDQ (1.13 g, 4.98 mmol) was then added, and the resulting mixture was stirred for an additional 1 h. After being quenched with triethylamine, the reaction mixture was passed through an activated alumina column. The eluents were evaporated under reduced pressure to leave a solid residue, which was subjected to silica-gel column chromatography (hexane/CH_2Cl_2 = 2/1 to 1/1). The purple fraction (R_f = 0.36; hexane/CH_2Cl_2 = 2/1) was collected and evaporated under reduced pressure to afford **4H$_2$** as a purple crystalline solid (231 mg, 15%). Mp 240–242 °C. ^{1}H NMR ($CDCl_3$, 400 MHz): δ_H, ppm 8.90–8.88 (m, 8H), 8.09 (d, 4H, *J* = 1.6 Hz), 8.08 (d, 2H, *J* = 1.6 Hz), 7.83 (d, 1H, *J* = 7.6 Hz), 7.80 (d, 1H, *J* = 2.4 Hz), 7.79 (d, 2H, *J* = 2.0 Hz), 7.78 (d, 1H, *J* = 2.0 Hz), 7.63 (t, 1H, *J* = 8.0 Hz), 7.32 (ddd, 1H, *J* = 8.4, 2.6, 1.0 Hz), 3.98 (s, 3H), 1.523 (s, 36H), 1.518 (s, 18H), –2.71 (s, 2H). ^{13}C{^{1}H} NMR ($CDCl_3$, 100 MHz): δ_C, ppm 157.9, 148.7, 148.6, 143.8, 141.3, 141.2, 129.8, 129.7, 127.6, 127.4, 121.5, 121.4, 120.9, 120.3, 119.3, 113.5, 55.5, 35.0, 31.7. HRMS (ESI): m/z 981.6392 (calcd. for $C_{69}H_{81}N_4O$: 981.6405, $[M + H]^+$). UV/Vis (CH_2Cl_2): λ_{max}, nm (log ε) 420 (5.53), 517 (4.12), 553 (3.85), 591 (3.62), 647 (3.55).

5,10,15-Tris(3,5-di-tert-butylphenyl)-20-(3-methoxyphenyl)porphyrinatoplatinum(II) (4Pt). A mixture of **4H$_2$** (102 mg, 0.104 mmol), $Pt(acac)_2$ (131 mg, 0.333 mmol), and PhCN (20 mL) was heated at reflux for 37 h. The mixture was concentrated under reduced pressure to leave a solid residue, which was dissolved in CH_2Cl_2, washed with water, dried over Na_2SO_4, and evaporated under reduced pressure. The residue was subjected to silica-gel column chromatography (hexane/CH_2Cl_2 = 2/1), and the orange fraction (R_f = 0.33; hexane/CH_2Cl_2 = 5/1) was collected and evaporated to afford **4Pt** as an orange crystalline solid (111 mg, 91%). Mp > 300 °C. ^{1}H NMR ($CDCl_3$, 400 MHz): δ_H, ppm 8.82–8.78 (m, 8H), 8.02 (d, 4H, *J* = 1.6 Hz), 8.01 (d, 2H, *J* = 2.0 Hz), 7.77–7.75 (m, 4H), 7.72 (t, 1H, *J* = 2.6 Hz), 7.61 (t, 1H, *J* = 7.8 Hz), 7.30 (dd, 1H, *J* = 8.4, 2.6 Hz), 3.96 (s, 3H), 1.51 (s, 36H), 1.50 (s, 18H). ^{13}C{^{1}H} NMR ($CDCl_3$, 100 MHz): δ_C, ppm 158.0, 148.8, 142.9, 141.02, 140.97, 140.92, 140.6, 140.5, 130.93, 130.85, 130.77, 130.4, 129.1, 129.0, 127.6, 126.9, 123.6, 123.5, 121.5, 121.1, 119.5, 113.7, 55.5, 35.0, 31.7. HRMS (ESI): m/z 1174.5839 (calcd. for $C_{69}H_{79}N_4OPt$: 1174.5896, $[M + H]^+$). UV/Vis (CH_2Cl_2): λ_{max}, nm (log ε) 404 (5.50), 511 (4.42), 540 (3.01).

5,10,15-Tris(3,5-di-tert-butylphenyl)-20-(3-hydroxyphenyl)porphyrinatoplatinum(II) (5M). Typical procedure: To a solution of **4Pt** (46.8 mg, 0.0398 mmol) in CH_2Cl_2 (5 mL) was added BBr_3 (0.6 mL, 0.6 mmol) at –78 °C, and the mixture was stirred for 16 h at room temperature. After being quenched with a saturated $NaHCO_3$ solution, the aqueous layer was extracted with CH_2Cl_2, and the combined organic extracts were washed with water, dried over Na_2SO_4, and evaporated under reduced pressure. The residue was subjected to silica-gel column chromatography (hexane/CH_2Cl_2 = 1/1), and the orange fraction (R_f = 0.23; hexane/CH_2Cl_2 = 1/1) was collected and evaporated to afford **5Pt** as an orange crystalline solid (38.2 mg, 83%). Compound **5H$_2$** was similarly prepared in 99% yield from **4H$_2$** and BBr_3. **5Pt**: Mp 275–278 °C. ^{1}H NMR ($CDCl_3$, 400 MHz): δ_H, ppm 8.82–8.78 (m, 8H), 8.02–8.01 (m, 6H), 7.78 (d, 2H, *J* = 1.6 Hz), 7.77 (d, 1H, *J* = 2.4 Hz), 7.74 (d, 1H, *J* = 7.6 Hz), 7.63 (t, 1H, *J* = 2.0 Hz), 7.55 (t, 1H, *J* = 7.8 Hz), 7.18 (dd, 1H, *J* = 8.0, 2.6 Hz), 4.92 (s, 1H), 1.51 (s, 36H), 1.50 (s, 18H). ^{13}C{^{1}H} NMR ($CDCl_3$, 100 MHz): δ_C, ppm 154.0, 148.9, 143.2, 141.15, 141.08, 141.05, 140.59, 140.57, 131.08, 131.01, 130.92, 130.4, 129.2, 129.1, 127.9, 127.1, 123.8, 123.6, 121.28, 121.24, 121.18, 114.8, 35.1, 31.8. HRMS (ESI): m/z 1160.5681 (calcd. for $C_{68}H_{77}N_4OPt$: 1160.5740, $[M + H]^+$). UV/Vis (CH_2Cl_2): λ_{max}, nm (log ε) 404 (5.44), 511 (4.41), 540 (3.60). IR (ATR): ν, cm^{-1} 3490–3112 (OH). **5H$_2$**: ^{1}H NMR ($CDCl_3$, 400 MHz): δ_H, ppm 8.90 (s, 4H), 8.87 (d, 2H, *J* = 4.8 Hz), 8.85 (d, 2H, *J* = 4.8 Hz), 8.08 (d, 4H, *J* = 1.6 Hz), 8.07 (d, 2H, *J* = 2.0 Hz), 7.79–7.78 (m, 3H), 7.76 (d, 1H, *J* = 7.6 Hz), 7.58 (s, 1H), 7.51 (t, 1H, *J* = 7.8 Hz), 6.95 (d, 1H, *J* = 6.8 Hz), 4.87 (brs, 1H), 1.521 (s, 36H), 1.518 (s, 18H), –2.73 (s, 2H). HRMS (ESI): m/z 966.6136 (calcd. for $C_{68}H_{78}N_4O$: 966.6170, $[M]^+$). UV/Vis (CH_2Cl_2): λ_{max}, nm (log ε) 420 (5.58), 517 (4.11), 552 (3.83), 590 (3.65), 647 (3.57). IR (ATR): ν, cm^{-1} 3600–3300 (OH).

Methyl 3,5-bis(10-phenylanthracen-9-yl)benzoate (8). A mixture of **6** (444 mg, 1.51 mmol), **7** (1.07 g,

3.59 mmol), $Pd(PPh_3)_4$ (349 mg, 0.302 mmol), K_2CO_3 (1.11 g, 8.06 mmol), toluene (8 mL), MeOH (3 mL), and H_2O (3 mL) was stirred at 80 °C for 12 h. The mixture was dissolved in EtOAc, and the resulting organic solution was washed with water, dried over Na_2SO_4, and evaporated under reduced pressure. The residue was subjected to silica-gel column chromatography (hexane/CH_2Cl_2 = 5/1 to 1/1), and the blue fraction (R_f = 0.42; hexane/CH_2Cl_2 = 1/1) was collected and evaporated to afford **8** as a yellow crystalline solid (845 mg, 87%). Mp > 300 °C. ^{1}H NMR ($CDCl_3$, 400 MHz): δ_H, ppm 8 .41 (d, 2H, *J* = 1.6 Hz), 7.92 (d, 4H, *J* = 8.8 Hz), 7.86 (t, 1H, *J* = 1.6 Hz), 7.71 (d, 4H, *J* = 8.8 Hz), 7.64–7.50 (m, 8H), 7.47–7.43 (m, 6H), 7.38–7.34 (m, 4H), 3.95 (s, 3H). ^{13}C{^{1}H} NMR ($CDCl_3$, 100 MHz): δ_C, ppm 167.1, 139.8, 139.0, 138.9, 137.8, 135.4, 131.8, 131.3, 131.0, 129.94, 129.90, 128.48, 128.46, 127.6, 127.3, 126.5, 125.6, 125.1, 52.4. HRMS (ESI): m/z 640.2389 (calcd. for $C_{48}H_{32}O_2$: 640.2397, $[M]^+$). UV/Vis (CH_2Cl_2): λ_{max}, nm (log ε) 298 (4.43), 377 (4.31), 358 (4.10). IR (ATR): ν, cm^{-1} 1720 (C=O).

3,5-Bis(10-phenylanthracen-9-yl)benzoic acid (9). A mixture of **8** (801 mg, 1.25 mmol), KOH (333 mg, 5.75 mmol), H_2O (2.5 mL), and THF (5 mL) was stirred at 100 °C for 14 h. After being quenched with 12 M HCl, the aqueous layer was extracted with EtOAc, and the combined organic extracts were washed with water, dried over Na_2SO_4, and evaporated under reduced pressure to afford **9** as a yellow crystalline solid (705 mg, 90%). R_f = 0; hexane/CH_2Cl_2 = 1/1. Mp > 300 °C. ^{1}H NMR ($CDCl_3$, 400 MHz): δ_H, ppm 8.45 (s, 2H), 7.92–7.89 (m, 5H), 7.70 (d, 4H, *J* = 8.8 Hz), 7.63–7.53 (m, 6H), 7.49–7.41 (m, 8H), 7.35–7.31 (m, 4H). ^{13}C{^{1}H} NMR ($CDCl_3$, 100 MHz): δ_C, ppm 170.8, 140.0, 138.9, 137.9, 135.1, 132.4, 131.24, 131.25, 130.0, 129.92, 129.87, 128.5, 128.4, 127.6, 127.3, 126.4, 125.6, 125.1. HRMS (ESI): m/z 626.2230 (calcd. for $C_{47}H_{30}O_2$: 626.2240, $[M]^+$). UV/Vis (CH_2Cl_2): λ_{max}, nm (log ε) 398 (4.43), 377 (4.41), 358 (4.18). IR (ATR): ν, cm^{-1} 3060–2920 (OH), 1690 (C=O).

3,5-bis(10-phenylanthracen-9-yl)benzoyl azide (10). A mixture of **9** (46.1 mg, 0.0735 mmol), $SOCl_2$ (10 µL, 0.14 mmol), and CH_2Cl_2 (5 mL) was heated at 40 °C for 2 h. The mixture was concentrated under reduced pressure to leave a solid residue (acid chloride), which was then dissolved in THF (6 mL). The resulting solution was slowly added to a H_2O solution (3 mL) of NaN_3 (60.9 mg, 0.937 mmol) at 0 °C. The mixture was stirred for 3 h at 0 °C followed by the addition of water. The aqueous layer was extracted with EtOAc, and the combined organic extracts were washed with water, dried over Na_2SO_4, and evaporated under reduced pressure. The residue was subjected to silica-gel column chromatography (hexane/CH_2Cl_2 = 2/1), and the blue-emitting fraction (R_f = 0.19; hexane/CH_2Cl_2 = 2/1) was collected and evaporated under reduced pressure to afford a yellow solid (34 mg) containing **10** as the major component. Compound **10** could not be separated from an unidentified side product, although the structure of **10** was characterized by the following spectral data. The yellow solid containing **10** was used for the next reaction without further purification. ^{1}H NMR ($CDCl_3$, 400 MHz): δ_H, ppm 8.40 (d, 2H, *J* = 1.6 Hz), 7.92 (t, 1H, *J* = 1.6 Hz), 7.88 (d, 4H, *J* = 8.8 Hz), 7.72 (d, 4H, *J* = 8.8 Hz), 7.64–7.55 (m, 6H), 7.51–7.42 (m, 9H), 7.39–7.35 (m, 4H). HRMS (ESI): m/z 651.2306 (calcd. for $C_{47}H_{29}N_3O$: 651.2305, $[M]^+$). IR (ATR): ν, cm^{-1} 2136 (C=O).

Anthracene-appended Pt-porphyrin (11M). Typical procedure: A mixture of **5Pt** (29.5 mg, 0.0254 mmol), crude **10** (ca. 34 mg, ca. 0.052 mmol), Et_3N (10 µL, 0.072 mmol), and toluene (5 mL) was heated at 110 °C for 4 h in a Schlenk tube. The mixture was then evaporated under reduced pressure, and the solid residue was subjected to silica-gel column chromatography (hexane/CH_2Cl_2 = 6/1 to 1/3). The orange fraction (R_f = 0.35; hexane/CH_2Cl_2 = 1/1) was collected and evaporated to afford **11Pt** as an orange crystalline solid (23.0 mg, 76%). Compound **11H$_2$** was similarly prepared in 13% yield from **5H$_2$** and **10**. **11Pt**: ^{1}H NMR ($CDCl_3$, 400 MHz): δ_H, ppm 8.80–8.76 (m, 8H), 8.02–7.98 (m, 12H), 7.85 (s, 2H), 7.76–7.75 (m, 3H), 7.71–7.67 (m, 5H), 7.62–7.54 (m, 7H), 7.48 (d, 2H, *J* = 7.2 Hz), 7.43–7.40 (m, 7H), 7.34–7.30 (m, 5H), 1.50 (s, 18H), 1.490 (s, 18H), 1.485 (s, 18H). HRMS (ESI): m/z 1783.7964 (calcd. for $C_{115}H_{105}N_5O_2Pt$: 1783.7944, $[M]^+$). UV/Vis (CH_2Cl_2): λ_{max}, nm (relative intensity) 405 (1), 511 (0.086), 540 (0.011). IR (ATR): ν, cm^{-1} 3393 (NH), 3060 (NH), 1749 (C=O). A reliable ^{13}C NMR spectrum of **11Pt** could not be obtained due to the gradual decomposition of **11Pt** in solution under the measurement conditions (for 5–6 h at room temperature under room light). **11H$_2$**: ^{1}H NMR ($CDCl_3$, 400 MHz): δ_H, ppm 8.90–8.88 (m, 8H), 8.10–8.06 (m, 7H), 8.02 (d, 4H, *J* = 8.8 Hz), 7.87 (br-s, 2H), 7.783–7.778 (m, 3H), 7.69–7.67 (m, 4H), 7.61–7.54 (m, 9H), 7.50–7.48 (m, 3H), 7.44–7.40 (m, 6H), 7.34–7.30 (m, 5H), 1.51 (s, 54H), –2.73 (s, 2H). HRMS (ESI): m/z 1591.8543 (calcd. for $C_{115}H_{108}N_5O_2$: 1591.8531, $[M + H]^+$). UV/Vis (CH_2Cl_2): λ_{max}, nm (relative intensity) 376 (0.075), 420 (1), 517 (0.032), 553 (0.015), 591 (0.0068), 647 (0.0056). IR (ATR): ν, cm^{-1} 3311 (NH), 3066 (NH), 1749 (C=O).

Phenyl (3,5-bis(10-phenylanthracen-9-yl)phenyl)-carbamate (12). A mixture of phenol (53.9 mg, 0.573 mmol), **10** (70.2 mg, 0.108 mmol), Et_3N (50 µL, 0.359 mmol), and toluene (5 mL) was heated at 110 °C for 4 h in a Schlenk tube. The mixture was then evaporated under reduced pressure, and the solid residue was subjected to silica-gel column chromatography (hexane/CH_2Cl_2 = 2/1 to 1/1). The blue-emitting fraction (R_f = 0.16; hexane/CH_2Cl_2 = 1/1) was collected and evaporated to afford **12** as a yellow solid (46.0 mg, 59%). Mp 192–196 °C. ^{1}H NMR ($CDCl_3$, 400 MHz): δ_H, ppm 8.03 (d, 4H, *J* = 8.8 Hz), 7.81 (s, 2H), 7.69 (d, 4H, *J* = 8.8 Hz), 7.63–7.52 (m, 6H), 7.51–7.43 (m, 9H), 7.38–7.33 (m, 6H), 7.23–7.18 (m, 4H). ^{13}C{^{1}H} NMR ($CDCl_3$,

100 MHz): δ_C, ppm 151.7, 150.5, 140.4, 139.0, 137.9, 137.6, 136.0, 131.4, 130.4, 130.0, 129.9, 129.4, 128.5, 127.6, 127.2, 126.8, 125.8, 125.4, 125.1, 121.7, 121.1. HRMS (ESI): m/z 717.2661 (calcd. for $C_{53}H_{35}NO_2$: 717.2662, $[M]^+$). UV/Vis (CH_2Cl_2): λ_{max}, nm (log ε) 398 (4.42), 377 (4.40), 358 (4.17). IR (ATR): ν, cm^{-1} 3399 (NH), 3060 (NH), 1753(C=O).

CV and DPV measurements

Electrochemical measurements were performed at room temperature on a CH Instruments model 650E electrochemical workstation using a conventional three-electrode cell. For the measurements in CH_2Cl_2, a glassy carbon working electrode, a Pt wire counter electrode, and an Ag/Ag^+ [0.01 M $AgNO_3$, 0.1 M Bu_4NPF_6 (MeCN)] reference electrode were used. Bu_4NPF_6 (in CH_2Cl_2) was used as a supporting electrolyte. The sample solutions were deoxygenated by bubbling with argon gas before the scan. The scan rate was 60 mV s^{-1} and the potentials are reported vs. ferrocene/ferrocenium as an external reference for the CH_2Cl_2 solutions.

Computational details

The geometries of the conformers A and B of **11Pt-m**, in which the *meso*-3,5-di-*tert*-butylphenyl groups of **11Pt** were replaced by phenyl groups, were optimized using the DFT method with the solvent effects incorporated by the polarizable continuum model (PCM) [19]. The basis sets used the 6-31G(d,p) basis set [20] for H, C, N, and O, and the LanL2DZ basis set (with effective core potentials) [21] for Pt. The function of DFT was the Becke, three-parameter, Lee–Yang–Parr (B3LYP) exchange-correlation functional [22]. We confirmed that the optimized geometries were not in the saddle but in stable points. The optimized geometries and energies are summarized in Table S1 in the Supporting Information. The electronic transition energies of **11Pt-m** were calculated by the TD-DFT method The basis sets and the function for the TD-DFT method were the same as those for the DFT method. To determine approximate rotation barriers at the carbazole linkage, we calculated the potential energies of 24 conformers of **11Pt-m** by rotating the C–O–C=O torsion angle by 15° while leaving the rest of the backbone unchanged (Fig. S2). All the calculations were carried out using the Gaussian 16 suite of programs [23].

Fluorescence measurements. Attempts to observe TTA-UC

Dichloromethane solutions of (a) **11Pt**/**12** (20/400 μM), (b) **4Pt**/DPA (20/400 μM), (c) PtOEP/**12** (20/400 μM), (d) PtOEP/DPA (20/400 μM), and (e) **11Pt** (20 μM) were prepared and bubbled with argon for 30 min. The PL spectra of these deaerated solutions were measured at 25 °C with selective excitation at the Q band using proper monochromatic lights. The excitation lights with the wavelengths of 511 nm and 535 nm were used respectively for (a), (b), and (e) and for (c) and (d). A short-cut optical filter of 490 nm was also set between the light source for excitation and the sample solutions to block unexpected stray light from the light source. The fluorescence in the short wavelength region was not detected by self-quenching due to the conc. DPA or DPA chromophore.

Phosphorescence lifetime measurements

Phosphorescence lifetime was determined by fitting phosphorescence decay by a single exponential function. The decays of the Pt-porphyrin-derived phosphorescence for **4Pt** and **11Pt** in deaerated CH_2Cl_2 were measured by a photomultiplier tube (HAMAMATSU, R7400U-01). A nanosecond pulse laser with a wavelength of 532 nm, a power of 134 μJ/pulse, and a repetition frequency of 100 Hz (CryLas, FDSS 532-150-I) was used as a light source to excite the Q-band of the samples. To detect only the phosphorescence from the sample, we put a notch filter to cut the scattered light of 532 nm and proper band-pass filters that passed the phosphorescence only at the peak wavelengths just before the photomultiplier tube.

Acknowledgments

This work was supported by JSPS KAKENHI (Grant Numbers: 21H04576 and 22H02061 to YM, 21K04980 to HN, 23H03945 to TI) and research grants from Uchida Energy Science Promotion Foundation and Union Tool Scholarship Society (TI).

Supporting information

Additional data are given in the supplementary material. This material is available free of charge *via* the Internet at https://www.worldscientific.com/doi/suppl/10.1142/S1088424623500840.

REFERENCES

1. (a) Singh-Rachford TN and Castellano FN. *Coord. Chem. Rev*. 2010; **254**: 2560–2573. (b) Zhou J, Liu Q, Feng W, Sun W and Li F. *Chem. Rev*. 2015; **115**: 395–465. (c) Yanai N and Kimizuka N. *Chem. Commun*. 2016; **52**: 5354–5370. (d) Askes SHC and Bonnet S. *Nat. Rev. Chem*. 2018; **2**: 437–452. (e) Bharmoria P, Bildirir H and Moth-Poulsen K. *Chem. Soc. Rev*. 2020; **49**: 6529–6554, and references therein.
2. For example, see: (a) Cheng YY, Fückel B, MacQueen RW, Khoury T, Clady RGCR, Schulze TF, Ekins–Daukes NJ, Crossley MJ, Stannowski B, Lips K and Schmidt TW. *Energy Environ. Sci*. 2012; **5**: 6953–6959. (b) Monguzzi A, Braga D, Gandini

M, Holmberg VC, Kim DK, Sahu A, Norris DJ and Meinardi F. *Nano Lett*. 2014; **14**: 6644–6650. (c) Schulze TF and Schmidt TW. *Energy Environ. Sci*. 2015; **8**: 103–125. (d) Hill SP, Dilbeck T, Baduell E and Hanson K. *ACS Energy Lett*. 2016; **1**: 3–8. (e) Dilbeck T and Hanson K. *J. Phys. Chem. Lett*. 2018; **9**: 5810–5821. (f) Morifuji T, Takekuma Y and Nagata M. *ACS Omega* 2019; **4**: 11271–11275.

3. For example, see: (a) Ravetz BD, Pun AB, Churchill EM, Congreve DN and Rovis T. *Nature* 2019; **565**: 343–346. (b) Yu T, Liu Y, Zeng Y, Chen J, Yang G and Li Y. *Chem. Eur. J*. 2019; **25**: 16270–16276. (c) Huang L, Wu W, Li Y, Huang K, Zeng L, Lin W and Han G. *J. Am. Chem. Soc*. 2020; **142**: 18460–18470.
4. For example, see: (a) Wohnhaas C, Turshatov A, Mailänder V, Lorenz S, Baluschev S, Miteva T and Landfester K. *Macromol. Biosci*. 2011; **11**: 772–778. (b) Park YI, Lee KT, Suh YD and Hyeon T. *Chem. Soc. Rev*. 2015; **44**: 1302–1317. (c) Huang L, Zhao Y, Zhang H, Huang K, Yang J and Han G. *Angew. Chem. Int. Ed*. 2017; **56**: 14400–14404. (d) Sasaki Y, Oshikawa M, Bharmoria P, Kouno H, Hayashi-Takagi A, Sato M, Ajioka I, Yanai N and Kimizuka N. *Angew. Chem. Int. Ed*. 2019; **58**: 17827–17833.
5. For example, see: (a) Park J, Xu M, Li F and Zhou HC. *J. Am. Chem. Soc*. 2018; **140**: 5493–5499. (b) Hamblin MR. *Dalton Trans*. 2018; **47**: 8571–8580. (c) Dartar S, Ucuncu M, Karakus E, Hou Y, Zhao J and Emrullahoglu M. *Chem. Commun.* 2021; **57**: 6039–6042.
6. (a) Kimizuka N, Yanai N and Morikawa M. *Langmuir* 2016; **32**: 12304–12322. (b) Yanai N and Kimizuka N. *Acc. Chem. Res*. 2017; **50**: 2487–2495. (c) Yanai N and Kimizuka N. *Angew. Chem. Int. Ed*. 2020; **59**: 10252–10264.
7. Covalently linked anthracene–porphyrin dyads: (a) Ezoe M, Minami T, Ogawa Y, Yagi S, Nakazumi H, Matsuyama T, Wada K and Horinaka H. *Photochem. Photobiol. Sci*. 2005; **4**: 641–646. (b) Sudha K, Sundharamurthi S, Karthikaikumar S, Abinaya K and Kalimuthu P. *J. Phys. Chem. C* 2017; **121**: 5941–5948. (c) Liu S, Wang X, Liu H, Shen L, Zhao D and Li X. *J. Mater. Chem. C* 2020; **8**: 3536–3544.
8. Covalently linked anthracene–anthracene oligomers and polymers: (a) Dzebo D, Börjesson K, Gray V, Moth-Poilsen K and Albinsson B. *J. Phys. Chem. C* 2016; **120**: 23397–23406. (b) Edhborg F, Bildirir H, Bharmoria P, Moth-Poulsen K and Albinsson B. *J. Phys. Chem. B* 2021; **125**: 6255–6263.
9. Anthracene–porphyrin coordination complexes: (a) Gray V, Börjesson K, Dzebo D, Abrahamsson M, Albinsson B and Moth-Poulsen K. *J. Phys. Chem. B* 2016; **120**: 19018–19026. (b) Edhborg F, Küçüköz B, Gray V and Albinsson B. *J. Phys. Chem. B* 2019; **123**: 9934–9943.
10. Covalently linked anthracene–anthracene dyads: (a) Matsui Y, Kanoh M, Ohta E, Ogaki T and Ikeda H. *J. Photochem. Photobio. A* 2020; **387**: 112107. (b) Olesund A, Gray V, Mårtensson J and Albinsson B. *J. Am. Chem. Soc.* 2021; **143**: 5745–5754.
11. Covalently linked bisanthracene–porphyrin triads: (a) Day S, Mondal P and Rath SP. *New J. Chem*. 2015; **39**: 4100–4108. (b) Tanaka K, Ohashi W, Inafuku K, Shiotsu S and Chujo Y. *Dyes Pigments* 2020; **172**: 107821.
12. Covalently linked anthracene–porphyrin nanorods: Xu Y, Gsänger S, Minameyer MB, Imaz I, Maspoch D, Shyshov O, Schwer F, Ribas X, Drewello T, Meyer B and von Delius M. *J. Am. Chem. Soc.* 2019; **141**: 18500–18507.
13. Differential pulse voltammetry of **12** revealed that the 2e-oxidation of the BPAB unit proceeded as a two-step, one-electron process with a slight potential separation of 0.056 V. This indicates that the electronic interaction between the two anthracene units through the phenylene bridge cannot be ignored for the reference BPAB.
14. Brinen JS and Koren JG. *Chem. Phys. Lett*. 1968; **2**: 671–672.
15. Drouet S, Paul-Roth CO, Fattori V, Cocchi M and Williams JAG. *New J. Chem*. 2011; **35**: 438–444.
16. Fazio MA, Durandin A, Tkachenko NV, Niemi M, Lemmetyinen H and Schuster DI. *Chem. Eur. J*. 2009; **15**: 7698–7705.
17. Kavali RR, Lee BC, Moon BS, Yang SD, Chun KS, Choi CW, Lee CH and Chi DY. *J. Label. Compd. Radiopharm*. 2005; **48**: 749–758.
18. Newman SG and Lautens M. *J. Am. Chem. Soc*. 2010; **132**: 11416–11417.
19. Cancès E, Mennucci B and Tomasi J. *J. Chem. Phys.* 1997; **107**: 3032–3041.
20. (a) Hehre WJ, Ditchfield R and Pople JA. *J. Chem. Phys.* 1972; **56**: 2257–2261. (b) Francl MM, Petro WJ, Hehre WJ, Binkley JS, Gordon MS, DeFrees DJ and Pople JA. *J. Chem. Phys.* 1982; **77**: 3654–3665.
21. Wadt WR and Hay PJ. *J. Chem. Phys.* 1985; **82**: 284–298.
22. (a) Becke AD. *J. Chem. Phys.* 1988; **98**: 5648–5652. (b) Lee C, Yang W and Parr RG. *Phys. Rev. B* 1988; **37**: 785–789.
23. Frisch MJ, Trucks GW, Schlegel HB, Scuseria GE, Robb MA, Cheeseman JR, Scalmani G, Barone V, Petersson GA, Nakatsuji H, Li X, Caricato M, Marenich AV, Bloino J, Janesko BG, Gomperts R, Mennucci B, Hratchian HP, Ortiz JV, Izmaylov AF, Sonnenberg JL, Williams-Young D, Ding F, Lipparini F, Egidi F, Goings J, Peng B, Petrone A, Henderson T, Ranasinghe D, Zakrzewski VG, Gao J, Rega N, Zheng G, Liang W, Hada M, Ehara

M, Toyota K, Fukuda R, Hasegawa J, Ishida M, Nakajima T, Honda Y, Kitao O, Nakai H, Vreven T, Throssell K, Montgomery JA Jr, Peralta JE, Ogliaro F, Bearpark MJ, Heyd JJ, Brothers EN, Kudin KN, Staroverov VN, Keith TA, Kobayashi R, Normand J, Raghavachari K, Rendell AP, Burant JC, Iyengar SS, Tomasi J, Cossi M, Millam JM, Klene M, Adamo C, Cammi R, Ochterski JW, Martin RL, Morokuma K, Farkas O, Foresman JB and Fox DJ. *Gaussian 16*, Revision C.01, Gaussian, Inc., Wallingford CT, 2019.